Ninth International Conference on
THIN-WALLED STRUCTURES – ICTWS2023
Sydney, Australia, Nov 29 – Dec 1, 2023

# EXPERIMENTAL INVESTIGATION OF COLD-FORMED STEEL BUILT-UP CLOSED SECTION BEAM-COLUMNS UNDER MOMENT GRADIENTS

**Qiu-Yun Li and Ben Young**

Department of Civil and Environmental Engineering, The Hong Kong Polytechnic University, Hong Kong, China
e-mails: qiuyun.li@polyu.edu.hk, ben.young@polyu.edu.hk

**Keywords**: Beam-columns; Buckling behaviour; Built-up sections; Cold-formed steel; Moment gradients; Non-uniform bending.

**Abstract**. *An experimental program is presented in this paper to examine the behaviour of cold-formed steel built-up closed section beam-columns under moment gradients. In total, eighteen eccentric compression tests were conducted on the cold-formed steel built-up closed section members between pin-ended supports. A combination of compression and non-uniform minor axis bending was applied to the test specimens by implementing unequal loading eccentricities at two ends of the members. The end moment ratios ranging between -1.0 and 1.0 were considered to explore the effect of non-uniform bending on the strengths of thin-walled built-up closed section beam-columns. The test results in terms of loading capacity, failure mode and axial load-lateral deflection response were obtained. Furthermore, based on nominal resistances against pure compression and pure bending calculated by direct strength method, the applicability of the interaction formulae specified in the AISI S100, AS/NZS 4600 and ANSI/AISC 360 was evaluated for the cold-formed steel built-up closed section members subjected to synchronous compression and non-uniform minor axis bending.*

## 1 INTRODUCTION

For the convenience of brake-pressing or cold-rolling, traditional cold-formed steel (CFS) members are commonly manufactured with point- or singly-symmetric cross-sections, which are prone to failing by twisting or torsion. One cost-effective way to enhance the torsional stability of CFS components is to assemble two or more individual sections by welds, bolts or self-tapping screws to form built-up closed sections or doubly-symmetric open sections. Due to their great potential in providing superior loading capacities, CFS built-up section members have aroused widespread research interests over the past decade [1, 2]. Up to now, the existing studies have mainly contributed to acquiring the knowledge of CFS built-up section members under simple loading condition such as pure bending [3-6] or pure compression [7-11]. However, most structural elements in actual buildings are subjected to combined loading. For instance, beam-column members that experience synchronous compressive load and bending moment are essential components as usually found in structures. In practice, non-uniform moment distributions along the member length are found for beam-columns, as induced by unequal end moments or transverse forces. In the modern standards [12-14], the influence of non-uniform bending on the member strength is considered by adopting the equivalent uniform moment factor ($C_m$). The conception of "equivalent moment" was originally put forward to utilize the sinusoidal bending distribution to replace the actual first order moment [15]. For beam-columns under linear bending distributions along the member length, the theoretical expression of $C_m$ includes the effects of end moment ratio and relative axial strength ratio, as provided in the DIN 18800 [16]. For the purpose of handier calculation, a simple formula that account for the effect of end moment ratio was derived by Austin [17] to approximately

determine $C_m$ and is adopted in the international design specifications [12-14]. The widely accepted formula of $C_m$ [17] was initially proposed for non-slender section members. For thin-walled section components susceptible to complex buckling failures, the applicability of equivalent moment method should be evaluated.

An experimental program, which has been presented by Li and Young [18], is described in this paper to investigate the performance of CFS built-up closed section beam-columns experiencing moment gradients. The built-up sections consisted of two stiffened channels were brake-pressed from zinc-coated steel sheets of grades G500 and G550. Self-tapping screws were employed to compose the built-up section members and discretely distributed along the member length. A total of eighteen specimens were tested under eccentric compression. Unequal loading eccentricities were applied at two ends of the specimens to induce a combination of compression and non-uniform minor axis bending. Two nominal plate thicknesses of 0.75 and 1.2 mm as well as two nominal member lengths of 900 and 1500 mm were devised for the built-up closed section specimens to constitute four test series. For each test series, a wide spectrum of end moment ratios ranging between -1.0 and 1.0 was incorporated to examine the influence of moment gradients on the stability of CFS built-up section beam-columns. The minutiae of test specimens, initial global imperfection measurements, arrangement of test setup and experimental results were reported. Furthermore, underpinned by the loading capacities obtained from the tests, the appropriateness of the interaction formulae as stipulated in the North American Specification [12], Australian/New Zealand Standard [13] and American Specification [14] together with nominal pure compression and pure bending resistances predicted by direct strength method was assessed for the thin-walled built-up closed section beam-columns under moment gradients.

## 2 EXPERIMENTAL PROGRAM

### 2.1 Test specimens

This experimental program was performed on CFS built-up closed section members experiencing synchronous compression and non-uniform minor axis bending. One type of built-up section configuration was formed by assembling two identical channels (parts “a” and “b”) face-nesting, which was designated as CW-section and is illustrated in Figure 1. The self-tapping screws with nominal diameter and nominal length of 4.8 and 12.5 mm, respectively, were located at the middle of the overlapped elements of the built-up section and discretely distributed along the member length to fasten two individual components as an entirety. A general fastener spacing of 100 mm that fulfilled the provision specified in Clause 4.1.2 of the AS/NZS 4600 [13] was arranged along the longitudinal direction of all the specimens in this test program, while a finer spacing of 20 mm was utilized at both ends of the CFS built-up closed section members.

To explore the buckling behaviour of the CW-section beam-columns under moment gradients, two nominal plate thicknesses of 0.75 and 1.2 mm as well as two nominal member lengths of 900 and 1500 mm were considered in this study. Four series of eccentric compression tests consisting of eighteen CW-section beam-columns were conducted between pin-ended supports. Before connecting by self-tapping screws, the dimensions of the CW-section specimens were measured for individual channel components (parts “a” and “b”), as summarized in Table 1. The label system was defined for the test specimens to exhibit the information of cross-sectional profile, nominal plate thickness and nominal member length. For example, the label “CW-T1.2L1500A” represents the CW-section specimen with nominal plate thickness and nominal member length of 1.2 and 1500 mm, respectively. The letters of “A” to “E” at the end of the labels denote the varying end moment ratios of each test series.

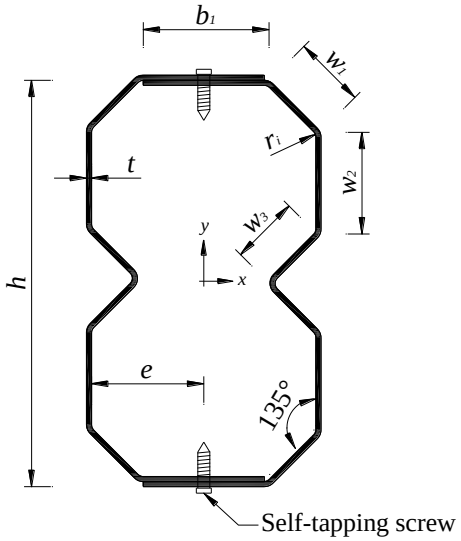


Figure 1: Cross-section configuration and symbol definition of CW-section.

Table 1: Measured dimensions of CFS built-up CW-section specimens [18].

| Specimen | Part | $h$ (mm) | $w_1$ (mm) | $w_2$ (mm) | $w_3$ (mm) | $b_1$ (mm) | $t$ (mm) | $t^*$ (mm) | $e$ (mm) | $r_i$ (mm) |
|---|---|---|---|---|---|---|---|---|---|---|
| CW-T0.75L900A | a | 102.4 | 14.4 | 30.7 | 14.0 | 29.8 | 0.793 | 0.748 | 25.1 | 1.5 |
| | b | 103.0 | 14.6 | 30.9 | 14.0 | 30.3 | 0.792 | 0.747 | 25.5 | 1.5 |
| CW-T0.75L900B | a | 102.4 | 14.3 | 30.8 | 14.0 | 30.6 | 0.795 | 0.750 | 25.4 | 1.5 |
| | b | 102.0 | 14.4 | 30.5 | 14.0 | 30.5 | 0.794 | 0.749 | 25.4 | 1.5 |
| CW-T0.75L900C | a | 101.8 | 13.7 | 30.9 | 14.0 | 31.3 | 0.802 | 0.757 | 25.3 | 1.5 |
| | b | 101.4 | 14.3 | 30.5 | 13.7 | 31.0 | 0.800 | 0.755 | 25.6 | 1.5 |
| CW-T0.75L900D | a | 102.5 | 14.0 | 31.0 | 14.1 | 30.5 | 0.793 | 0.748 | 25.1 | 1.5 |
| | b | 103.0 | 14.3 | 31.0 | 14.1 | 30.6 | 0.789 | 0.744 | 25.4 | 1.5 |
| CW-T1.2L900A | a | 98.9 | 14.4 | 28.6 | 14.2 | 31.8 | 1.249 | 1.207 | 26.0 | 2.3 |
| | b | 99.2 | 14.2 | 28.9 | 14.2 | 31.4 | 1.247 | 1.205 | 25.8 | 2.3 |
| CW-T1.2L900B | a | 99.0 | 14.2 | 28.8 | 14.2 | 31.4 | 1.237 | 1.195 | 25.8 | 2.3 |
| | b | 99.8 | 14.4 | 29.0 | 14.3 | 31.4 | 1.238 | 1.196 | 25.9 | 2.3 |
| CW-T1.2L900C | a | 101.1 | 14.9 | 29.1 | 14.6 | 31.0 | 1.227 | 1.185 | 26.1 | 2.3 |
| | b | 100.7 | 14.7 | 29.1 | 14.5 | 31.5 | 1.228 | 1.186 | 26.2 | 2.3 |
| CW-T1.2L900D | a | 100.3 | 14.5 | 29.0 | 14.5 | 31.4 | 1.243 | 1.201 | 26.0 | 2.5 |
| | b | 101.4 | 14.6 | 29.5 | 14.5 | 31.7 | 1.245 | 1.203 | 26.2 | 2.5 |
| CW-T1.2L900E | a | 99.6 | 14.8 | 28.7 | 14.2 | 31.6 | 1.231 | 1.189 | 26.2 | 2.3 |
| | b | 99.7 | 14.5 | 29.1 | 14.0 | 31.3 | 1.232 | 1.190 | 25.9 | 2.3 |
| CW-T0.75L1500A | a | 104.6 | 14.4 | 31.4 | 14.6 | 30.5 | 0.796 | 0.751 | 25.4 | 1.5 |
| | b | 103.3 | 14.7 | 30.9 | 14.1 | 30.1 | 0.798 | 0.753 | 25.5 | 1.5 |
| CW-T0.75L1500B | a | 104.2 | 14.8 | 30.9 | 14.6 | 30.3 | 0.796 | 0.751 | 25.6 | 1.5 |
| | b | 102.9 | 14.1 | 30.9 | 14.4 | 30.4 | 0.799 | 0.754 | 25.2 | 1.5 |
| CW-T0.75L1500C | a | 102.8 | 14.6 | 30.9 | 13.8 | 30.2 | 0.792 | 0.747 | 25.4 | 1.5 |
| | b | 103.5 | 14.2 | 31.2 | 14.3 | 30.0 | 0.796 | 0.751 | 25.1 | 1.5 |
| CW-T0.75L1500D | a | 100.3 | 13.0 | 30.6 | 14.1 | 31.8 | 0.791 | 0.746 | 25.1 | 1.5 |
| | b | 102.7 | 14.4 | 30.8 | 14.1 | 30.6 | 0.786 | 0.741 | 25.5 | 1.5 |
| CW-T1.2L1500A | a | 101.5 | 14.5 | 29.5 | 14.7 | 31.2 | 1.243 | 1.201 | 25.9 | 2.5 |
| | b | 100.8 | 14.8 | 28.9 | 14.7 | 31.0 | 1.244 | 1.202 | 26.0 | 2.5 |
| CW-T1.2L1500B | a | 100.6 | 14.6 | 29.1 | 14.5 | 31.1 | 1.237 | 1.195 | 25.9 | 2.3 |
| | b | 101.3 | 14.2 | 29.6 | 14.7 | 30.8 | 1.240 | 1.198 | 25.5 | 2.3 |
| CW-T1.2L1500C | a | 102.1 | 14.8 | 29.3 | 15.1 | 30.3 | 1.233 | 1.191 | 25.6 | 2.5 |
| | b | 101.2 | 14.5 | 29.0 | 15.2 | 30.6 | 1.232 | 1.190 | 25.6 | 2.5 |
| CW-T1.2L1500D | a | 100.5 | 14.2 | 29.0 | 15.0 | 30.9 | 1.241 | 1.199 | 25.5 | 2.3 |
| | b | 101.0 | 14.6 | 29.0 | 14.9 | 30.7 | 1.245 | 1.203 | 25.7 | 2.3 |
| CW-T1.2L1500E | a | 99.7 | 14.3 | 28.8 | 14.6 | 30.9 | 1.241 | 1.199 | 25.6 | 2.3 |
| | b | 100.2 | 14.9 | 28.6 | 14.6 | 30.7 | 1.244 | 1.202 | 25.8 | 2.3 |

Note: $t^*$ = thickness of base metal.

## 2.2 Material properties

The folded-flange channel components of the CW-section specimens with nominal plate thicknesses of 0.75 and 1.2 mm were brake-pressed from G550 and G500 zinc-coated steel sheets, respectively. To account for the effect of cold-work, the tensile coupons, which were longitudinally extracted from the flat elements ($b_1$ and $w_2$) and the intermediate stiffeners (90-degree curved portions) of the channel sections, were tested to measure the actual material properties of the CW-section members. With the use of concentrated hydrochloric acid, the zinc-coatings within the gauge length of flat coupon specimens were removed before the tensile tests to determine the thickness of zinc-coating layers. The average thicknesses of single zinc-coating layer were measured as 0.023 and 0.021 mm [10] for the 0.75 and 1.2 mm thick steel sheets, respectively, which were utilized to calculate the thickness of base metal ($t$*) for the CW-section members, as displayed in Table 1. The material properties obtained from the longitudinal tensile coupon tests, which have been reported by Li and Young [10] for the same batch of test specimens, are listed in Table 2, where $E$ is the Young's modulus, $\sigma_{0.2}$ is the static 0.2% proof stress, $\sigma_u$ is the static ultimate tensile stress, and $\varepsilon_f$ is the strain at fracture.

Table 2: Material properties measured from tensile coupon tests [10].

| Coupon | | $E$ (GPa) | $\sigma_{0.2}$ (MPa) | $\sigma_u$ (MPa) | $\varepsilon_f$ (%) |
|---|---|---|---|---|---|
| Flat portion | CW-T0.75F-Flange | 216 | 611 | 620 | 9.2 |
| | CW-T0.75F-Web | 216 | 618 | 619 | 9.7 |
| | CW-T1.2F-Flange | 213 | 606 | 621 | 9.9 |
| | CW-T1.2F-Web | 212 | 608 | 623 | 9.1 |
| Curved portion | CW-T0.75C-Web | 224 | 631 | 644 | 4.1 |
| | CW-T1.2C-Web | 223 | 636 | 665 | 5.2 |

## 2.3 Initial global imperfection measurements

It is inevitable to introduce the initial geometric imperfections to CFS built-up section members in the manufacturing process of brake-pressing or connecting fasteners. In this study, the initial global imperfection about the minor axis was measured for each CW-section specimen. For the pin-ended beam-column, the distribution of its initial global imperfection was assumed as a sinusoidal mode. Prior to each eccentric compression test, the spatial positions of the junction of the intermediate stiffener ($w_3$) and the adjacent flat element ($w_2$) were obtained at mid-height and two ends of the beam-column member using a Leica total station. The datum line was constructed by connecting the coordinates measured at two ends of the member. Then, the deviation of the horizontal coordinate acquired at mid-height of the member from the datum line was regarded as the initial global imperfection ($\omega_g$) of the beam-column. The measured values of $\omega_g$ normalized by the corresponding member lengths ($L$) are exhibited in Table 3 for all the CW-section specimens, where the positive value denotes the initial global imperfection in the same direction as the specimen offset from the loading position at the bottom end, and vice versa.

## 2.4 Test setup and operation

In this experimental program, the CFS built-up closed section beam-columns were eccentrically loaded to induce simultaneous compression and minor axis bending. The non-uniform bending with linear moment distribution along the member length was generated by applying unequal initial loading eccentricities at the bottom and top ends of the beam-columns, as illustrated in Figure 2. For each test series, the nominal initial loading eccentricity at the bottom end ($e_0$) kept identical for all the specimens, whereas that at the top end ($\psi e_0$) changed for the specimens to cater for different values of end moment ratio ($\psi$) ranging between -1 and 1. According to the sign convention as prescribed in the European Code [19], the values of $\psi$

were taken as positive and negative for the moment distributions leading to single- and reverse-curvature bending, respectively.

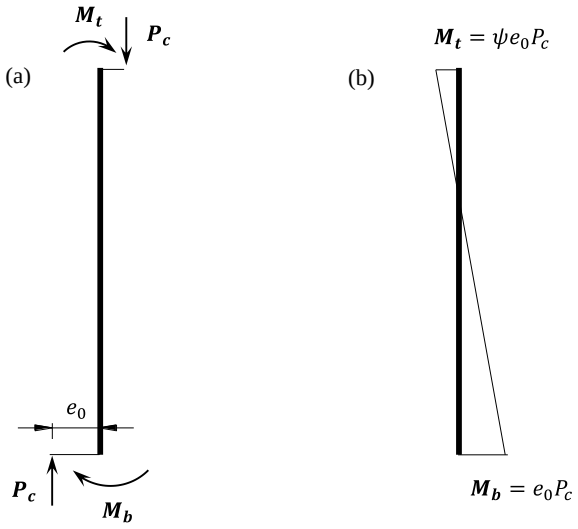


Figure 2: Schematic diagrams of beam-column member under moment gradients: (a) Combined loading diagram; (b) Bending moment diagram.

The arrangement of non-uniform bending beam-column test rig is shown in Figure 3. The specially designed assembly of V-shape pit plate with knife-edge plate, which released the rotation about the minor axis (*y*-*y*) but restrained the bending about the orthogonal axis (*x*-*x*) of the specimens, was employed to fulfill the pin-ended boundary condition. The upper pit plate was attached to the reaction frame and the lower pit plate together with a lockable ball bearing was set on the loading platform. When installing each specimen, a Leica total station was used to place the beam-column to a desired location with the target initial loading eccentricities at both ends of the member. Subsequently, the 16 mm thick end plates welded to the milled ends of the built-up section member were bolted to the wedge plates. It is noteworthy that the warping of the cross-sections at both ends of each specimen was restrained during the testing.

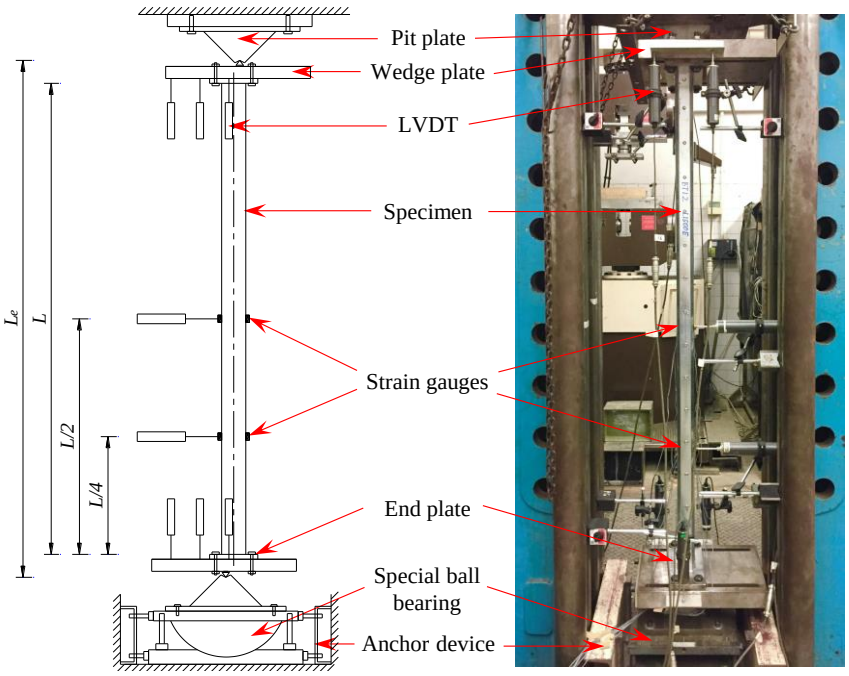


Figure 3: Arrangement of non-uniform bending beam-column test.

A hydraulic testing machine was utilized to conduct the beam-column tests. At the preloading stage, the unlocked ball bearing freely rotated to eliminate possible gaps of the entire test setup. Before formal loading, all the vertical and horizontal bolts were tightened to restrict the ball bearing from twisting, rotation, and any horizontal shift due to the reaction force caused by the unequal end moments. Two linear variable displacement transducers (LVDTs) were horizontally set at quarter- and mid-heights of each specimen to obtain the lateral deflections. At each wedge plate, three LVDTs were vertically installed to measure the end rotations of the beam-column. Moreover, four strain gauges were affixed onto the outer fibres of the member at quarter- and mid-heights each to capture the longitudinal strains. The displacement control with a loading rate of 0.2 mm/min was adopted for all the specimens. To preclude the influence of loading rate, two 100-second pauses were performed for each beam-column before and near the ultimate load to determine the static responses.

### 2.5 Determination of $e_0$ and $\psi$

The end moment ratio ($\psi$) was introduced in this study to describe the different cases of moment gradients, which was defined as $M_t/M_b$, where $M_t$ and $M_b$ are the bending moments at the top and bottom ends of the member, respectively. Within the elastic range, the moment of the beam-column member is represented by $EI_y\kappa$ based on compatibility of deformation, where $EI_y$ is the bending stiffness about the minor axis of the section and $\kappa$ is the bending curvature that was calculated in accordance with the longitudinal strains measured by the strain gauges, as detailed in Zhao et al. [20]. Meanwhile, the moment of any cross-section of the member can be obtained by computing the resultant moment of the reaction force at the bottom end support relative to the corresponding cross-section. According to equilibrium conditions of each specimen at quarter- and mid-heights, the values of initial loading eccentricity at the bottom end ($e_0$) and end moment ratio ($\psi$) were determined from Eq. (1) [20] and Eq. (2) [18], respectively, where $\Delta_{L/4}$ and $\Delta_{L/2}$ are the horizontal lateral deflections of the member at quarter- and mid-heights, respectively, $P_c$ is the applied compressive load, $L$ is the member length, and $L_e$ is the effective member length that was regarded as the vertical distance between the pinned ends, as illustrated in Figure 3. On the basis of a sinusoidal mode, the initial global imperfections of the beam-column specimens at quarter- and mid-heights ($\omega_{L/4}$ and $\omega_{L/2}$) equal to $\omega_g \sin[\pi(L_e/2 - L/4)/L_e]$ and $\omega_g$, respectively, where $\omega_g$ is the initial global imperfection measured at mid-height of the specimen.

$$e_0 = \frac{2L_e}{L}\left(\frac{EI_y\kappa_{L/4}}{P_c} - \omega_{L/4} - \Delta_{L/4}\right) - \frac{2L_e - L}{L}\left(\frac{EI_y\kappa_{L/2}}{P_c} - \omega_{L/2} - \Delta_{l/2}\right) \quad (1)$$

$$\psi = \frac{2}{e_0}\left(\frac{EI_y\kappa_{L/2}}{P_c} - \omega_{L/2} - \Delta_{L/2}\right) - 1 \quad (2)$$

### 2.6 Experimental results

In this study, failure modes of the CFS built-up closed section beam-columns under moment gradients were observed at the ultimate loads. For the CW-section members with relatively slender cross-sections (i.e., test series CW-T0.75L900 and CW-T0.75L1500), the majority of the specimens failed by the interaction of local buckling at the overlapped plates, inward distortional buckling at the intermediate stiffener and overall flexural buckling (L+D+F), as exemplified in Figure 4 for a typical specimen CW-T0.75L900C. For test series CW-T1.2L900 and CW-T1.2L1500 with relatively compact cross-sections, the loading capacities of all the specimens were dominated by the local-flexural interaction (L+F). The local buckling half-waves of the CW-section beam-columns formed at the overlapped plates between the adjacent screws, which evidenced that the arrangement of self-tapping screws had an influence on the

behaviour of the CFS built-up CW-section members under synchronous compression and non-uniform minor axis bending.

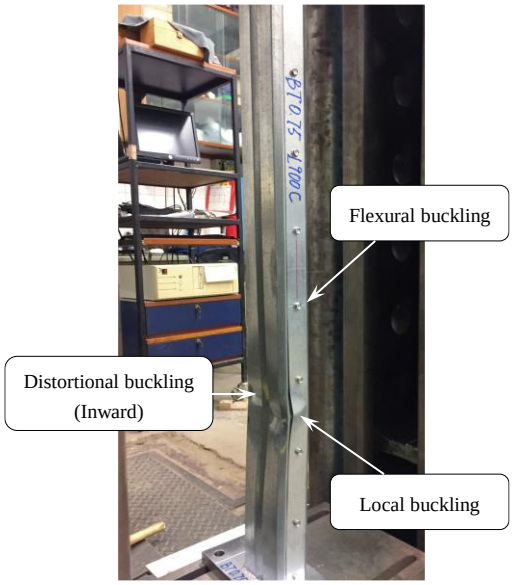


Figure 4: Failure mode of test specimen CW-T0.75L900C.

The static axial load versus mid-height lateral deflection responses of test series CW-T1.2L1500 are exhibited in Figure 5. The experimental results including failure mode, measured initial loading eccentricity at the bottom end ($e_0$), measured end moment ratio ($\psi$), loading capacity ($P_{Exp}$), and moment at the bottom end ($M_{Exp,b}$) corresponding to the ultimate load that was calculated by $e_0 P_{Exp}$ are summarized in Table 3 for all the CW-section beam-columns experiencing non-uniform bending. Compared to the specimen with the greatest end moment ratio in the same test series, the loading capacity of the CW-section specimen with the smallest end moment ratio increased by 18% on average in this experimental program. It indicated that the non-uniform bending had a beneficial effect on the strengths of the CFS built-up CW-section beam-columns, which may result from the increasing of bending strain energy when the normalized deflection shape of the member changed from a half sinusoidal wave ($\psi$ = 1.0) to a full sinusoidal wave ($\psi$ = -1.0).

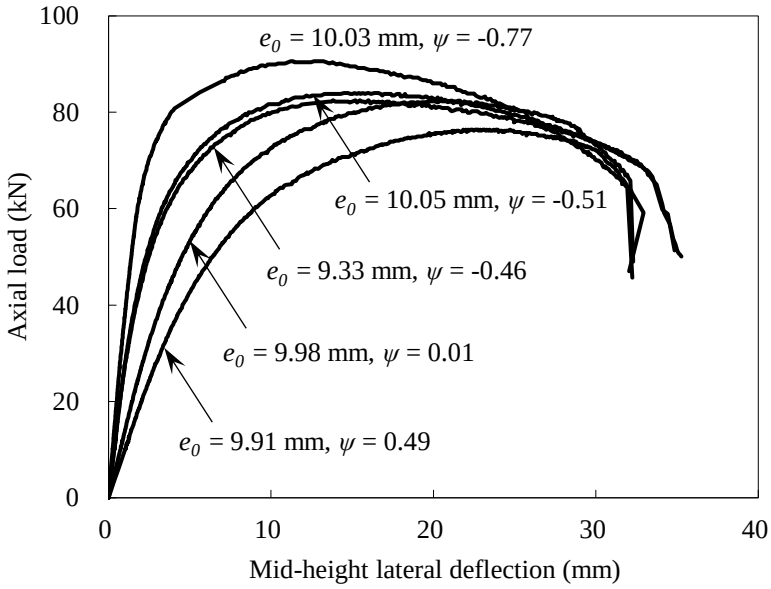


Figure 5: Axial load-lateral deflection responses of test series CW-T1.2L1500 [18].

Table 3: Experimental results and comparison with strength predictions [18].

| Specimen | Failure mode | $\frac{\omega_g}{L}$ | $e_0$ (mm) | $\psi$ | $P_{Exp}$ (kN) | $M_{Exp.b}$ (kNmm) | $\frac{P_{Exp}}{P_{AISI}}$ | $\frac{P_{Exp}}{P_{AS/NZS}}$ | $\frac{P_{Exp}}{P_{AISC}}$ |
|---|---|---|---|---|---|---|---|---|---|
| CW-T0.75L900A | L+D+F | 1/1549 | 8.16 | 0.80 | 49.8 | 406.4 | 0.86 | 0.86 | 0.83 |
| CW-T0.75L900B | L+D+F | -1/1549 | 9.28 | 0.39 | 53.9 | 500.2 | 0.91 | 0.91 | 0.88 |
| CW-T0.75L900C | L+D+F | 1/1549 | 8.93 | -0.15 | 63.1 | 563.5 | 0.94 | 0.94 | 0.91 |
| CW-T0.75L900D | L+F | 1/1772 | 9.46 | -0.79 | 65.1 | 615.8 | 0.88 | 0.88 | 0.87 |
| CW-T1.2L900A | L+F | 1/7087 | 8.66 | 0.43 | 118.5 | 1026.2 | 1.06 | 1.06 | 1.03 |
| CW-T1.2L900B | L+F | 1/2362 | 8.83 | 0.12 | 120.0 | 1059.6 | 1.04 | 1.04 | 1.01 |
| CW-T1.2L900C | L+F | -1/7087 | 8.47 | 0.06 | 119.6 | 1013.0 | 1.01 | 1.01 | 0.98 |
| CW-T1.2L900D | L+F | 1/1549 | 9.58 | -0.38 | 124.7 | 1194.6 | 0.99 | 0.99 | 0.96 |
| CW-T1.2L900E | L+F | -1/1549 | 8.37 | -0.73 | 129.6 | 1084.8 | 0.95 | 0.95 | 0.93 |
| CW-T0.75L1500A | L+D+F | 1/2830 | 10.15 | 0.40 | 42.1 | 427.3 | 1.04 | 1.04 | 1.01 |
| CW-T0.75L1500B | L+D+F | 1/5906 | 9.08 | 0.13 | 44.9 | 407.7 | 1.05 | 1.05 | 1.03 |
| CW-T0.75L1500C | L+D+F | 1/3937 | 11.68 | -0.36 | 47.4 | 553.6 | 1.12 | 1.12 | 1.09 |
| CW-T0.75L1500D | L+D+F | 1/2953 | 10.86 | -0.75 | 48.3 | 524.5 | 1.04 | 1.04 | 1.02 |
| CW-T1.2L1500A | L+F | -1/7853 | 9.91 | 0.49 | 76.4 | 757.1 | 1.15 | 1.15 | 1.12 |
| CW-T1.2L1500B | L+F | -1/3937 | 9.98 | 0.01 | 82.5 | 823.4 | 1.19 | 1.19 | 1.16 |
| CW-T1.2L1500C | L+F | 1/3371 | 9.33 | -0.46 | 82.5 | 769.7 | 1.12 | 1.12 | 1.10 |
| CW-T1.2L1500D | L+F | 1/3371 | 10.05 | -0.51 | 84.0 | 844.2 | 1.12 | 1.12 | 1.10 |
| CW-T1.2L1500E | L+F | 1/5906 | 10.03 | -0.77 | 90.6 | 908.7 | 1.15 | 1.15 | 1.13 |
| Mean ($P_m$) | - | - | - | - | - | - | 1.03 | 1.03 | 1.01 |
| COV ($V_P$) | - | - | - | - | - | - | 0.095 | 0.095 | 0.097 |
| Resistance factor ($\phi$) | - | - | - | - | - | - | 0.85 | 0.85 | 0.90 |
| Reliability index ($\beta$) | - | - | - | - | - | - | 2.56 | 2.35 | 2.23 |

Note: L = local buckling; D = distortional buckling; F = flexural buckling.

## 3 DESIGN OF BEAM-COLUMNS UNDER MOMENT GRADIENTS

### 3.1 General

In the modern design specifications [12-14], various axial load-moment interaction relationships are available for the strength check of beam-column members, which are generally anchored to the nominal resistances against pure compression and pure bending. For the built-up CW-sections with longitudinal stiffeners, direct strength method (DSM) that avoids the cumbersome calculation of effective cross-sectional properties and considers complex buckling modes is a favorable design approach. Therefore, codified DSM equations were adopted in this study to determine the nominal pure compression and pure bending resistances of the CW-section beam-columns subjected to unequal end moments. The critical elastic buckling strengths that are essential in the DSM equations were obtained utilizing the advanced finite strip analysis program CUFSM [21] based on the solid blocks model proposed by Li and Young [10]. In this study, the applicability of the typical linear, two-stage and bi-linear axial load-moment interaction expressions specified in the North American Specification [12], Australian/New Zealand Standard [13] and American Specification [14], respectively, together with the nominal pure compression and pure bending resistances calculated by DSM was examined for the CFS built-up CW-section beam-columns. Moreover, the effect of moment gradients on the loading capacities of structural members is involved in the current design codes by introducing the equivalent uniform moment factor ($C_m$). For linear moment distributions along the member length, the approximate equation proposed by Austin [17], as presented in Eq. (3), is stipulated in the aforementioned design specifications [12-14] and was thus adopted in this study to compute the equivalent uniform moment factor ($C_m$).

$$C_m = 0.6 + 0.4\psi \tag{3}$$

where $\psi$ is the end moment ratio.

Furthermore, the reliability analysis was performed to evaluate the applicability of the existing design rules for the CFS built-up closed section members experiencing synchronous compression and non-uniform minor axis bending. The reliability index ($\beta$) with the prescribed minimum value taken as 2.5 was calculated from Eq. K2.1.1-2 of the AISI S100 [12]. The fabrication and material parameters were incorporated in the reliability analysis by using the mean values of $F_m$ = 1.00 and $M_m$ = 1.05 with the corresponding coefficients of variation (COVs) of $V_F$ = 0.05 and $V_M$ = 0.10, as suggested in Table K2.1.1-1 of the AISI Specification [12]. The typical dead load (DL) and live load (LL) combinations of 1.2DL+1.6LL, 1.2DL+1.5LL and 1.2DL+1.6LL were employed for the AISI S100 [12], AS/NZS 4600 [13] and ANSI/AISC 360 [14], respectively, based on the dead-to-live ratio of 1/5. The resistance factors ($\phi$) specified in the aforementioned design codes [12-14] were used in the determination of $\beta$. Additionally, the influence due to a limited number of test data was considered by the calibration parameter ($C_P$), as acquired from Eq. K2.1.1-4 of the AISI S100 [12].

### 3.2 North American Specification [12]

The interaction relationship expressed by Eq. (4) is stipulated in Clause H1.2 of the AISI S100 [12] for strength predictions of CFS beam-columns. In accordance with Clause C1.2.1.1 of the AISI Specification [12], the required second order flexural strength ($M_{nd}$) in Eq. (4) was obtained by the amplification of the first order elastic bending moment ($M_{nt}$) to take account of the *P*-$\delta$ effect, as denoted by Eq. (5), in which the equivalent uniform moment factor ($C_m$) is included. The expression of Eq. (3) is recommended in the AISI S100 [12] to calculate $C_m$ for beam-columns not subjected to transverse loading. In addition, the nominal resistances against pure compression ($P_n$) and pure bending ($M_n$) in Eq. (4) were obtained according to the DSM equations provided in Chapters E and F of the AISI Specification [12], respectively. It is worthwhile to mention that the modified slenderness ratio of the CW-section members was acquired from Eq. I1.2-1 of the AISI S100 [12] and used in the computation of $P_n$ to consider the slip-effect between individual components connected by discrete self-tapping screws.

$$\frac{P}{P_n}+\frac{M_{nd}}{M_n}\leq 1.0 \tag{4}$$

$$M_{nd}=\frac{C_m M_{nt}}{1-P/P_{cr}} \tag{5}$$

where *P* is the required compressive strength and $P_{cr}$ is the critical elastic buckling strength of the member in the plane of bending.

According to the design provisions specified in the AISI S100 [12], the nominal compressive strengths ($P_{AISI}$) were determined for the CFS built-up CW-section beam-columns under moment gradients and compared with the experimental loading capacities ($P_{Exp}$), as shown in Table 3 and Figure 6, where $P_{Pred}$ represents the predicted nominal compressive strength. For the eighteen CW-section members, the mean value and COV of $P_{Exp}/P_{AISI}$ equal to 1.03 and 0.095, respectively. Based on the resistance factor ($\phi$) taken as 0.85, the calculated $\beta$ of 2.56 was larger than the prescribed minimum value of 2.5. The results indicated that the interaction formula in the North American Specification [12] together with $P_n$ and $M_n$ determined by DSM as well as $C_m$ calculated from Eq. (3) could reliably provide overall conservative strength predictions for the CFS built-up closed section members experiencing synchronous compression and non-uniform minor axis bending.

### 3.3 Australian/New Zealand Standard [13]

The segmented expression of Eq. (6) addressed in Clause 3.5.1 of the AS/NZS 4600 [13] was assessed for the CFS built-up section beam-columns under moment gradients. It is worth

noting that the required second order flexural strength ($M_{nd}$) that incorporates the effect of non-uniform bending, as displayed in Eq. (5), was only adopted for $P/P_n$ > 0.15, otherwise the maximum first order bending moment ($M_{nt}$) was directly used in the interaction formula. The expression of Eq. (3) is also employed in the AS/NZS 4600 [13] to calculate the equivalent uniform moment factor ($C_m$). The nominal resistances of $P_n$ and $M_n$ in Eq. (6) were determined by the DSM equations as stipulated in Clause 7.2 of the AS/NZS 4600 [13]. Moreover, the modified slenderness ratio calculated from Eq. 4.1.2 of the Australian/New Zealand Standard [13] was utilized to obtain the nominal pure compression resistance ($P_n$) of the built-up section members to account for the shear rigidity reduction.

$$\frac{P}{P_n} + \frac{M_{nd}}{M_n} \leq 1.0 \quad \text{for} \quad \frac{P}{P_n} > 0.15 \tag{6a}$$

$$\frac{P}{P_n} + \frac{M_{nt}}{M_n} \leq 1.0 \quad \text{for} \quad \frac{P}{P_n} \leq 0.15 \tag{6b}$$

The results in Table 3 reveal that the mean value of test-to-predicted strength ratio ($P_{Exp}/P_{AS/NZS}$) equal to 1.03 for the eighteen CW-section members with the corresponding COV of 0.095. Additionally, the calculated value of $\beta$ was 2.35 based on the resistance factor ($\phi$) of 0.85, which was less than the target value of 2.5. Overall, the two-stage interaction formula of Eq. (6) specified in the AS/NZS 4600 [13] together with the codified DSM to calculate $P_n$ and $M_n$ as well as Eq. (3) to obtain the equivalent uniform moment factor ($C_m$) conservatively and unreliably predicted the strengths of the CFS built-up closed section beam-columns under moment gradients.

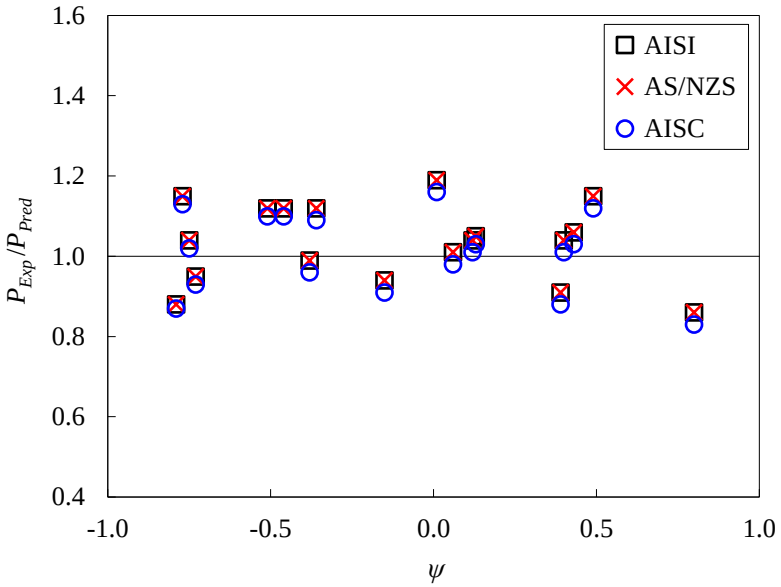


Figure 6: Comparison of experimental loading capacities with strength predictions.

### 3.4 American Specification [14] using direct strength method

The bi-linear interaction expression of Eq. (7) is suggested in Clause H1 of the ANSI/AISC 360 [14] for the design of beam-column members. The required second order flexural strength ($M_{nd}$) in Eq. (7) was obtained from Eq. (5), which considers the effect of moment gradients by the equivalent uniform moment factor ($C_m$). The formula of Eq. (3) is prescribed in the American Specification [14] to determine $C_m$ for beam-columns not subjected to transverse loading. Moreover, the DSM equations and relevant provisions provided in Chapters E and F of the AISI S100 [12] were employed to calculate the nominal pure compression and pure

bending resistances ($P_n$ and $M_n$) of the CW-section beam-columns. The comparison of experimental loading capacities ($P_{Exp}$) with the nominal compressive strengths ($P_{AISC}$) is displayed in Table 3 and Figure 6. For the eighteen CW-section members, the mean value and COV of $P_{Exp}/P_{AISC}$ were 1.01 and 0.097, respectively, with the calculated $\beta$ of 2.23 that was smaller than the lower bound of 2.5. Therefore, it manifested that the nominal strengths predicted by the interaction formula specified in the ANSI/AISC 360 [14] together with the nominal resistances of $P_n$ and $M_n$ determined by DSM as well as the equivalent uniform moment factor ($C_m$) acquired from Eq. (3) were overall slightly conservative for the CFS built-up closed section beam-columns experiencing non-uniform bending, which were found to be unreliable based on the resistance factor ($\phi$) of 0.90.

$$\frac{P}{P_n}+\frac{8}{9}\frac{M_{nd}}{M_n}\leq 1.0 \quad \text{for} \quad \frac{P}{P_n}\geq 0.2 \tag{7a}$$

$$\frac{P}{2P_n}+\frac{M_{nd}}{M_n}\leq 1.0 \quad \text{for} \quad \frac{P}{P_n}< 0.2 \tag{7b}$$

## 4 CONCLUSIONS

The experimental study was carried out to investigate the behaviour of cold-formed steel (CFS) built-up closed section beam-columns under moment gradients. The built-up closed (CW) sections were composed of two stiffened channels brake-pressed from G500 and G550 zinc-coated steel sheets. In this test program, the nominal plate thicknesses of 0.75 and 1.2 mm as well as nominal member lengths of 900 and 1500 mm were devised for the CW-section specimens. A total of eighteen eccentric compression tests were conducted on the CFS built-up closed section beam-columns between pin-ended supports. A combination of compression and non-uniform minor axis bending was induced to the test specimens by applying unequal loading eccentricities at two ends of the members. The measured values of end moment ratio ($\psi$) ranging from -0.79 to 0.80 were involved in this study to examine the influence of moment gradients on the strengths of the thin-walled built-up CW-section beam-columns. It was observed in the experimental program that all the CW-section specimens with nominal plate thickness of 1.2 mm failed by the local-flexural interaction (L+F), while the interaction of local, distortional and flexural buckling (L+D+F) was found for most of the specimens with nominal plate thickness of 0.75 mm. Compared to the specimens with the greatest end moment ratios in the same test series, the experimental loading capacities of the CW-section specimens with the smallest end moment ratios increased by average of 18% in this study, which evidenced the beneficial effect of non-uniform bending on the strengths of the CFS built-up closed section beam-columns. Furthermore, underpinned by the loading capacities obtained from the tests, it was revealed that the axial load-moment interaction formulae specified in the AISI S100 [12], AS/NZS 4600 [13] and ANSI/AISC 360 [14] together with the nominal resistances against pure compression and pure bending determined by direct strength method as well as the equivalent uniform moment factor calculated from Eq. (3) generally provided slightly conservative strength predictions for the CFS built-up CW-section members experiencing synchronous compression and non-uniform minor axis bending.

## REFERENCES

[1] Rasmussen K.J.R., Khezri M., Schafer B.W. and Zhang H., "The mechanics of built-up cold-formed steel members", *Thin-walled Structures*, **154**, 106756, 2020.

[2] Meza F.J., Becque J. and Hajirasouliha I., "Experimental study of cold-formed steel built-up beams"; *Journal of Structural Engineering*, **146**, 04020126, 2020.

[3] Wang L. and Young B., "Beam tests of cold-formed steel built-up sections with web perforations", *Journal of Constructional Steel Research*, **115**, 18-33, 2015.

[4] Li Y.-L., Li Y.-Q. and Shen Z.-Y., "Investigation on flexural strength of cold-formed thin-walled steel beams with built-up box section", *Thin-Walled Structures*, **107**, 66-79, 2016.

[5] Selvaraj S. and Madhavan M., "Structural design of cold-formed steel face-to-face connected built-up beams using direct strength method", *Journal of Constructional Steel Research*, **160**, 613-628, 2019.

[6] Li Q.-Y. and Young B., "Structural performance of cold-formed steel built-up section beams under non-uniform bending", *Journal of Constructional Steel Research*, **189**, 107050, 2022.

[7] Reyes W. and Guzmán A., "Evaluation of the slenderness ratio in built-up cold-formed box sections", *Journal of Constructional Steel Research*, **67**, 929-935, 2011.

[8] Zhang J.-H. and Young B., "Experimental investigation of cold-formed steel built-up closed section columns with web stiffeners", *Journal of Constructional Steel Research*, **147**, 380-392, 2018.

[9] Meza F.J., Becque J. and Hajirasouliha I., "Experimental study of cold-formed steel built-up columns", *Thin-Walled Structures*, **149**, 106291, 2020.

[10] Li Q.-Y. and Young B., "Experimental and numerical investigation on cold-formed steel built-up section pin-ended columns", *Thin-Walled Structures*, **170**, 108444, 2022.

[11] Abbasi M., Rasmussen K.J.R., Khezri M. and Schafer B.W., "Experimental investigation of the sectional buckling of built-up cold-formed steel columns", *Journal of Constructional Steel Research*, **203**, 107803, 2023.

[12] AISI, North American specification for the design of cold-formed steel structural members, *AISI S100-16*, American Iron and Steel Institute, Washington, 2016.

[13] AS/NZS, Design of cold-formed steel structures, *AS/NZS 4600: 2018*, Standards Australia and Standards New Zealand, Sydney, Australia, 2018.

[14] ANSI/AISC, Specification for structural steel buildings, *ANSI/AISC 360-16*, American National Standards Institute and American Institute of Steel Construction, Chicago, 2016.

[15] Boissonnade N., Jaspart J.-P., Muzeau J.-P. and Villette M., "New interaction formulae for beam-columns in Eurocode 3: The French–Belgian approach", *Journal of Constructional Steel Research*, **60**, 421-431, 2004.

[16] DIN, Steel structures - Part 1: design and construction, *DIN 18800-1*, German Institute for Standardisation (Deutsches Institut für Normung), Berlin, Beuth Verlag, 1988.

[17] Austin W., "Strength and design of metal beam-columns", *Journal of the Structural Division*, **87**, 1-34, 1961.

[18] Li Q.-Y. and Young B., "Experimental study on cold-formed steel built-up section beam-columns experiencing non-uniform bending", *Engineering Structures*, **256**, 113954, 2022.

[19] CEN, Design of steel structures. Part 1-1: General rules and rules for buildings, *EN 1993-1-1*, European Committee for Standardization, Brussels, Belgium, 2005.

[20] Zhao O., Gardner L. and Young B., "Experimental study of ferritic stainless steel tubular beam-column members subjected to unequal end moments", *Journal of Structural Engineering*, **142**, 04016091, 2016.

[21] Schafer B.W. and Ádány S., "Buckling analysis of cold-formed steel members using CUFSM: conventional and constrained finite strip methods", *Proceedings of the 18th International Specialty Conference on Cold-Formed Steel Structures*, Orlando, Florida, USA, 2006.